Semaphorin 3E and Plexin-D1 Control Vascular Pattern Independently of Neuropilins

Chenghua Gu, *et al.*

Science **307**, 265 (2005);
DOI: 10.1126/science.1105416

molecular structure of the $A\beta_{1-40}$ protofilament (*13*, *15*). STEM, ^{15}N-^{13}C coupling, and chemical shift data for quiescent $A\beta_{1-40}$ fibrils indicate a qualitatively different structure in both molecular conformation and supramolecular organization. The largest chemical shift differences, suggesting the largest conformational differences, occur at Q15 and in residues 22 to 28. Although all residues in agitated $A\beta_{1-40}$ fibril samples exhibit one major set of ^{13}C chemical shifts (with the exception of D23, V24, and K28, possibly indicating the coexistence of two distinct D23-K28 salt bridge geometries), many residues in quiescent fibril samples exhibit two sets of ^{13}C chemical shifts, with an approximate 2:1 ratio of NMR signal intensities (e.g., I31 side-chain signals in Fig. 2). This observation raises the possibility that the quiescent $A\beta_{1-40}$ protofilament contains two structurally equivalent and one structurally inequivalent subunits, consistent with Fig. 4, B and C.

We point out four physical and biological implications of these data. First, the sensitivity of fibril morphology and molecular structure to growth conditions shows that at least two distinct fibril nucleation mechanisms exist for $A\beta_{1-40}$. One mechanism, leading to quiescent fibrils, may be purely homogeneous. The other mechanism, leading to agitated fibrils, may depend on the interface between the peptide solution and the air or the walls of the sample tube. The molecular structure of $A\beta_{1-40}$ fibrils is not determined solely by amino acid sequence and is not purely under thermodynamic control. Second, the phenomenon of strains in prion diseases, in which a single prion protein gives rise to multiple, distinct phenotypes, has been attributed to an ability of both mammalian and yeast prion proteins to adopt multiple, distinct amyloid-like structures. Observed differences in proteolysis patterns (*22*, *23*), resistance to chemical denaturation (*24*), seeding efficiencies (*25*), and electron paramagnetic resonance signals (*26*) support this proposal, but clear connections between morphological variations and molecular-level structural variations, between strains and morphological variations, and between strains and specific features of molecular structure have not yet been established experimentally. The correlations of amyloid fibril morphology with specific structural features established by our data, the demonstration of their self-propagating nature, and the observation of different neurotoxicities for different morphologies further strengthen the case for a structural origin of prion strains. Third, the importance of mature amyloid fibrils as etiological agents in AD and other amyloid diseases, as opposed to nonfibrillar oligomers observed at earlier stages of peptide incubation (*27*–*30*), is a subject of current controversy. One principal argument against a primary role for mature fibrils in AD has been the absence of a robust correlation between the severity of neurological impairment and the extent of amyloid deposition (*2*, *31*). Data in Fig. 3 raise the possibility that certain amyloid morphologies may be more pathogenic than others in the affected organs of amyloid diseases, which would weaken the correlation between disease symptoms and total amyloid deposition. Fourth, amyloid fibrils may prove useful as structural and chemical templates for self-assembled, one-dimensional nanomaterials with novel electronic or optical properties (*4*, *5*). Because structural uniformity is a likely prerequisite in such applications, the self-propagation of molecular structure demonstrated above may be important for reliable fabrication of amyloid-based nanomaterials.

References and Notes

1. M. Sunde, C. C. Blake, *Q. Rev. Biophys.* **31**, 1 (1998).
2. B. Caughey, P. T. Lansbury, *Annu. Rev. Neurosci.* **26**, 267 (2003).
3. R. Tycko, *Curr. Opin. Struct. Biol.* **14**, 96 (2004).
4. T. Scheibel *et al.*, *Proc. Natl. Acad. Sci. U.S.A.* **100**, 4527 (2003).
5. M. Reches, E. Gazit, *Science* **300**, 625 (2003).
6. C. S. Goldsbury *et al.*, *J. Struct. Biol.* **130**, 217 (2000).
7. J. L. Jimenez *et al.*, *Proc. Natl. Acad. Sci. U.S.A.* **99**, 9196 (2002).
8. J. D. Harper, S. S. Wong, C. M. Lieber, P. T. Lansbury, *Chem. Biol.* **4**, 119 (1997).
9. Materials and methods are available as supporting material on *Science* Online.
10. Single-letter abbreviations for the amino acid residues are as follows: A, Ala; C, Cys; D, Asp; E, Glu; F, Phe; G, Gly; H, His; I, Ile; K, Lys; L, Leu; M, Met; N, Asn; P, Pro; Q, Gln; R, Arg; S, Ser; T, Thr; V, Val; W, Trp; and Y, Tyr.
11. P. T. Lansbury *et al.*, *Nature Struct. Biol.* **2**, 990 (1995).
12. T. S. Burkoth *et al.*, *J. Am. Chem. Soc.* **122**, 7883 (2000).
13. A. T. Petkova *et al.*, *Proc. Natl. Acad. Sci. U.S.A.* **99**, 16742 (2002).
14. J. J. Balbach *et al.*, *Biophys. J.* **83**, 1205 (2002).
15. O. N. Antzutkin, R. D. Leapman, J. J. Balbach, R. Tycko, *Biochemistry* **41**, 15436 (2002).
16. C. P. Jaroniec *et al.*, *Proc. Natl. Acad. Sci. U.S.A.* **101**, 711 (2004).
17. D. S. Wishart, D. A. Case, *Methods Enzymol.* **338**, 3 (2001).
18. G. Cornilescu, F. Delaglio, A. Bax, *J. Biomol. NMR* **13**, 289 (1999).
19. M. Torok *et al.*, *J. Biol. Chem.* **277**, 40810 (2002).
20. I. Kheterpal, A. Williams, C. Murphy, B. Bledsoe, R. Wetzel, *Biochemistry* **40**, 11757 (2001).
21. A. D. Williams *et al.*, *J. Mol. Biol.* **335**, 833 (2004).
22. R. A. Bessen, R. F. Marsh, *J. Virol.* **66**, 2096 (1992).
23. G. C. Telling *et al.*, *Science* **274**, 2079 (1996).
24. J. Safar *et al.*, *Nature Med.* **4**, 1157 (1998).
25. P. Chien, J. S. Weissman, *Nature* **410**, 223 (2001).
26. M. Tanaka, P. Chien, N. Naber, R. Cooke, J. S. Weissman, *Nature* **428**, 323 (2004).
27. R. Kayed *et al.*, *Science* **300**, 486 (2003).
28. G. Bitan *et al.*, *Proc. Natl. Acad. Sci. U.S.A.* **100**, 330 (2003).
29. H. A. Lashuel, D. Hartley, B. M. Petre, T. Walz, P. T. Lansbury, *Nature* **418**, 291 (2002).
30. M. Bucciantini *et al.*, *Nature* **416**, 507 (2002).
31. M. D. Kirkitadze, G. Bitan, D. B. Teplow, *J. Neurosci. Res.* **69**, 567 (2002).
32. C. P. Jaroniec, B. A. Tounge, J. Herzfeld, R. G. Griffin, *J. Am. Chem. Soc.* **123**, 3507 (2001).

Supporting Online Material
www.sciencemag.org/cgi/content/full/307/5707/262/DC1
Materials and Methods
Figs. S1 to S4
Tables S1 and S2

15 April 2004; accepted 16 November 2004
10.1126/science.1105850

Semaphorin 3E and Plexin-D1 Control Vascular Pattern Independently of Neuropilins

Chenghua Gu,[1,2]* Yutaka Yoshida,[3]* Jean Livet,[4] Dorothy V. Reimert,[1,2] Fanny Mann,[4] Janna Merte,[1,2] Christopher E. Henderson,[4] Thomas M. Jessell,[3] Alex L. Kolodkin,[1]† David D. Ginty[1,2]†

The development of a patterned vasculature is essential for normal organogenesis. We found that signaling by semaphorin 3E (Sema3E) and its receptor plexin-D1 controls endothelial cell positioning and the patterning of the developing vasculature in the mouse. Sema3E is highly expressed in developing somites, where it acts as a repulsive cue for plexin-D1–expressing endothelial cells of adjacent intersomitic vessels. Sema3E–plexin-D1 signaling did not require neuropilins, which were previously presumed to be obligate Sema3 coreceptors. Moreover, genetic ablation of Sema3E or plexin-D1 but not neuropilin-mediated Sema3 signaling disrupted vascular patterning. These findings reveal an unexpected semaphorin signaling pathway and define a mechanism for controlling vascular patterning.

The peripheral nervous system and its vasculature develop coordinately in part through common developmental cues. Semaphorins, a family of phylogenetically conserved cell-surface and secreted proteins, control neuronal cell migration and axon guidance (*1*–*3*). Certain membrane-bound semaphorins bind directly to receptors of the plexin family (*4*–*7*), but the class 3 secreted semaphorins (Sema3A to Sema3F, referred to collective-

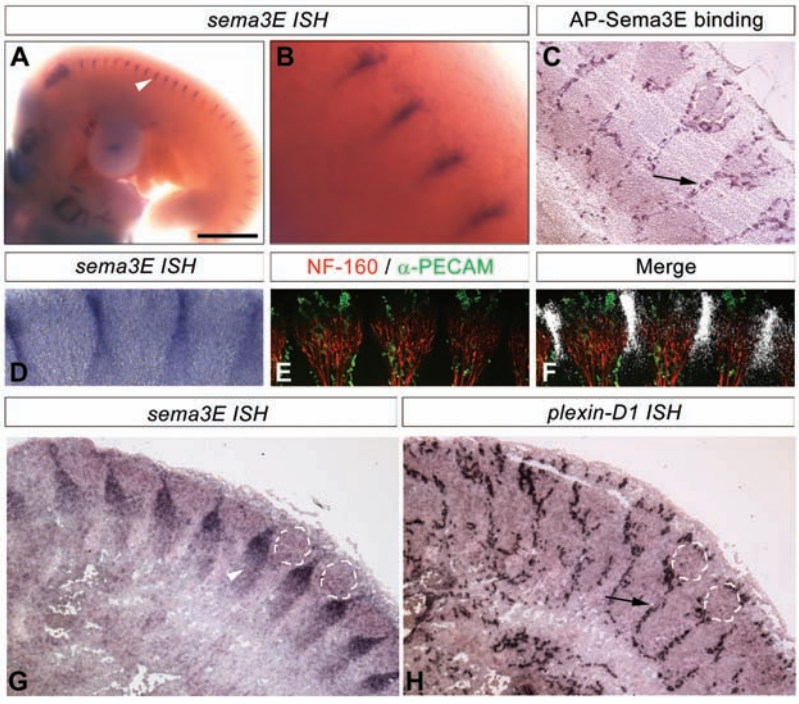

Fig. 1. Complementary expression patterns of *sema3E* in somites and *plexin-D1* and Sema3E binding sites on intersomitic blood vessels. (**A**) Whole-mount in situ hybridization (ISH) was performed on E11.5 embryos to visualize the pattern of expression of *sema3E*. In the trunk region, the highest level of Sema3E mRNA was detected in the caudal region of each somite. White arrowhead, region of *sema3E* mRNA expression. (**B**) High magnification of *sema3E* in situ hybridization shown in (A). (**C**) AP-Sema3E section binding to sagittal sections from E11.5 embryos. Black arrow, intersomitic vessels. (**D**) *Sema3E* in situ hybridization of a 100-μm-thick sagittal section of the E11.5 embryo shown in (A). (**E**) The embryo shown in (D) was immunostained with anti–platelet endothelial cell adhesion molecule (PECAM) (green) to visualize the vasculature and antineurofilament (red) to visualize spinal nerves and dorsal root ganglia (DRG). (**F**) Overlay of (D) and (E); *sema3E* mRNA [inversion of (D)], white; neurofilament, red; PECAM, green. (**G**) *Sema3E* in situ hybridization of an E11.5 embryo sagittal section. (**H**) *Plexin-D1* in situ hybridization of an E11.5 embryo sagittal section. White dotted lines outline the DRG. Scale bar, 1.2 mm (A); 300 μm [(B), (C), (G), and (H)]; 150 μm [(D) to (F)].

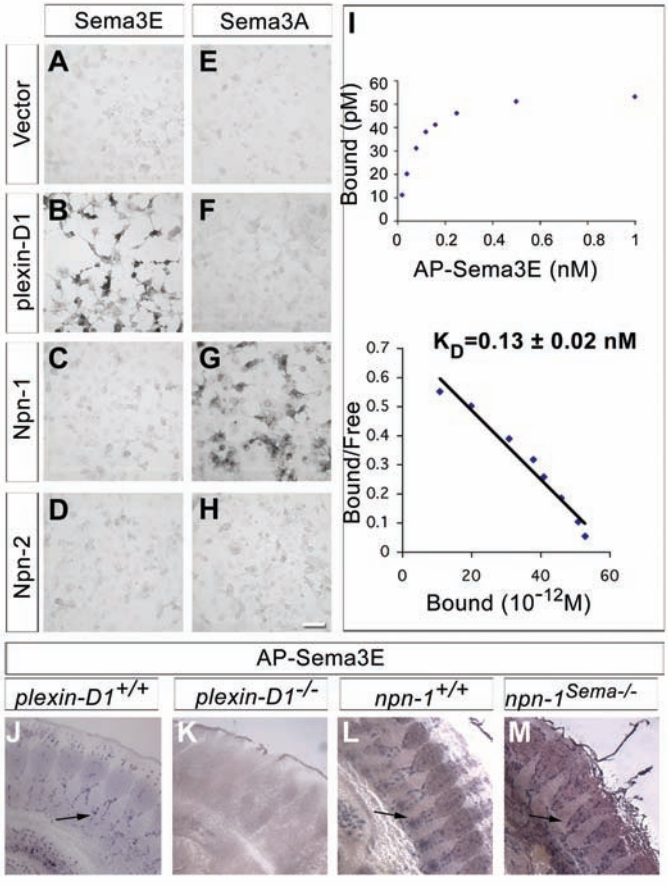

Fig. 2. Sema3E but not Sema3A binds with high affinity to plexin-D1, the endogenous receptor for Sema3E. (**A** to **D**) AP-Sema3E binds to COS-1 cells expressing plexin-D1 but not Npn-1 or Npn-2. (**E** to **H**) AP-Sema3A binds to COS-1 cells expressing Npn-1 but not plexin-D1 or Npn-2. COS-1 cells were transfected with either an empty vector [(A) and (E)] or an expression vector encoding plexin-D1 [(B) and (F)], Npn-1 [(C) and (G)], or Npn-2 [(D) and (H)]. Cells were incubated with either AP-Sema3E (0.5 nM) or AP-Sema3A (0.5 nM). (**I**) AP-Sema3E binding analysis reveals a tight association between AP-Sema3E and plexin-D1. The binding data were plotted by the method of Scatchard. The apparent K_D (±SEM) for the interaction between AP-Sema3E and plexin-D1 is 0.13 ± 0.02 nM (n = 8). (**J** and **K**) AP-Sema3E binds robustly to the vasculature in sections from wild-type (J) but not *plexin-D1*$^{-/-}$ (K) embryos. (**L** and **M**) Npn-1 is not an endogenous binding partner for Sema3E. AP-Sema3E binding to tissue sections prepared from E11.5 *npn-1*$^{Sema-/-}$ and wild-type littermate embryos. Black arrows, intersomitic vessels. Scale bar, 50 μm [(A) to (H)]; 60 μm [(J) to (M)].

ly as Sema3s) are thought to exert their effects exclusively through holoreceptor complexes that include neuropilin-1 (Npn-1) or Npn-2 and one of the four class A plexin proteins (*2*). Neuropilins function as the Sema3-binding subunits, whereas plexins serve as signal-transducing subunits. Neuropilins are also receptors for select isoforms of vascular endothelial growth factor (VEGF) family members (*8*–*12*). Thus, the severe cardiovascular defects observed in *npn-1* null mice (*13*) and the vascular defects resulting from overexpression of nonselective dominant-negative Npn's (*8*) could reflect a requirement for VEGF–Npn-1 signaling or Sema3–Npn-1 signaling. In vascular development, it is unclear whether Sema3s influence endothelial cell migration by binding to neuropilins, by antagonizing VEGF binding to neuropilins, or by acting through other signaling pathways.

To assess the contributions of Sema3s to vascular development, we focused on Sema3E because it is expressed in developing somites in the mouse (*14*) (Fig. 1, A, B, and G). We

[1]The Department of Neuroscience, [2]Howard Hughes Medical Institute, Johns Hopkins University School of Medicine, Baltimore, MD 21205–2185, USA. [3]Department of Biochemistry and Molecular Biophysics, Howard Hughes Medical Institute, Columbia University, New York, NY 10032, USA. [4]Institut National de la Santé et de la Recherche Médicale (INSERM), UMR623, Developmental Biology Institute of Marseille (IBDM), Marseille 13288, France.

*These authors contributed equally to this work.
†To whom correspondence should be addressed. E-mail: dginty@jhmi.edu (D.D.G.); kolodkin@jhmi.edu (A.L.K.)

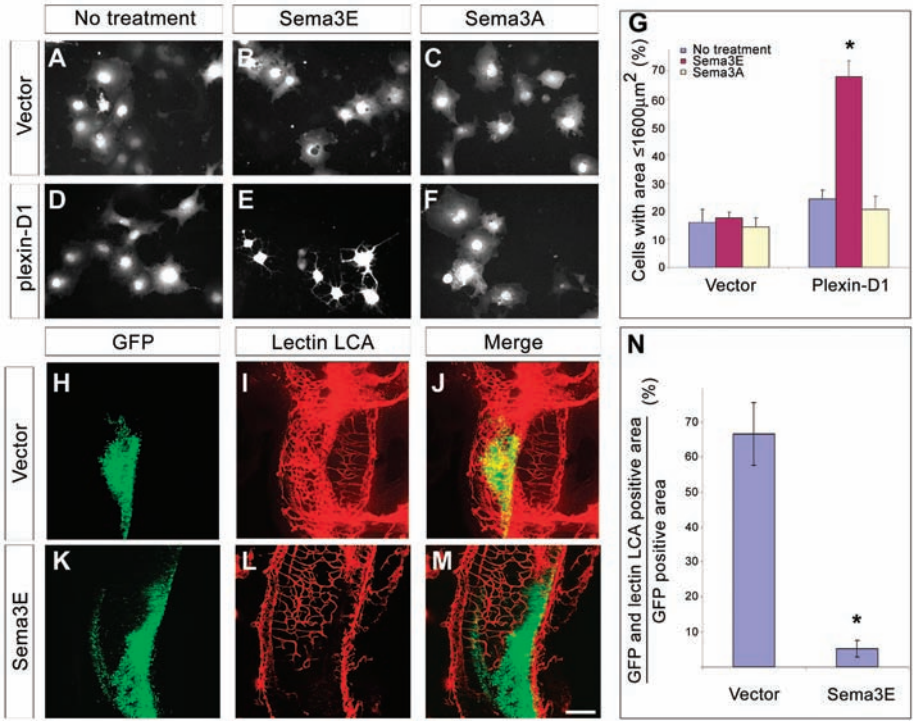

Fig. 3. Sema3E causes collapse of plexin-D1–expressing COS-7 cells and is a repellent for developing chick vasculature. (**A** to **F**) Plexin-D1–transfected COS-7 cells were incubated either with vehicle, Sema3E (AP-Sema3E; 0.1 to 0.5 nM), or Sema3A (AP-Sema3A; 1 to 2 nM). (**G**) COS-7 cell collapse was scored for 200 EGFP-positive cells for each experimental condition. A cell with a surface area less than 1600 μm² was considered collapsed (*17*). Shown are the means ± SEM (n = 5). Asterisk indicates statistical difference from all other groups ($P < 0.005$; analysis of variance with a Bonferroni post-hoc test). (**H** to **M**) An expression vector encoding EGFP (GFP) and either an empty vector [Vector, (H) to (J)] or a vector encoding Sema3E [(K) to (M)] were electroporated in ovo into E3 chicken embryos. Two days later, embryos were perfused with Lectin LCA, which binds to the vasculature. Lectin LCA (red) and EGFP (green) fluorescent signals were visualized by confocal microscopy. [(J) and (M)] Merges of Lectin LCA and EGFP signals. (**N**) Quantification of mean overlap (±SEM) between EGFP and Lectin LCA fluorescent signals in vector control and Sema3E electroporated embryos. EGFP alone, n = 7; EGFP + Sema3E, n = 9. Asterisk indicates statistical difference ($P < 0.001$, paired t test). Scale bar, 20 μm [(A) to (F)]; 200 μm [(H) to (M)].

compared the pattern of *sema3E* expression, assessed by in situ hybridization, with the pattern of endogenous Sema3E-binding partners, determined by binding of a chimeric alkaline phosphatase (AP)–Sema3E in embryonic tissues. In mouse embryos at embryonic day 10.5 (E10.5) and E11.5, *sema3E* expression was observed in the caudal region of each somite, immediately adjacent to the somite boundary and intersomitic blood vessels (Fig. 1, D to G, and fig. S1). In contrast, *sema3E* mRNA was not observed within the region of the somite containing the intersomitic blood vessels themselves (Fig. 1, D to G). However, AP-Sema3E binding sites were detected on the vasculature including the intersomitic vessels (Fig. 1C). Therefore, the expression of Sema3E and its endogenous receptor(s) suggests a role for Sema3E in patterning intersomitic vasculature.

The pattern of AP-Sema3E binding was markedly similar to the expression pattern of a plexin family member, plexin-D1, which localizes to the vasculature in mice (*9*) (Fig. 1H) and is critical for vascular development in both zebrafish and mice (*10*, *11*). In the trunk region of E10.5 and E11.5 mouse embryos, *plexin-D1* was expressed in intersomitic vessels adjacent to the caudal region of somites (Fig. 1, G and H, and fig. S1). To determine whether Sema3E binds to plexin-D1, AP-Sema3E was incubated with transfected COS cells (a monkey kidney cell line) expressing plexin-D1, Npn-1, or Npn-2. AP-Sema3E bound directly to plexin-D1 but to neither Npn-1 nor Npn-2 (Fig. 2, A to D). Moreover, Scatchard analysis revealed that the Sema3E–plexin-D1 interaction occurred at high affinity, with a dissociation constant (K_D) of 130 pM (Fig. 2I). Coexpression of Npn-1 or Npn-2 did not enhance the interaction between Sema3E and plexin-D1 (*15*). None of the other five Sema3s bound to plexin-D1, although four of those proteins (Sema3A, Sema3C, Sema3D, and Sema3F) bound directly to Npn-1, Npn-2, or both Npn's (Fig. 2, E to H, and fig. S2) (*15*). Sema3B at a concentration of 1.1 nM did not bind to either Npn-1 or Npn-2 (*15*).

To determine whether plexin-D1 is an endogenous receptor that mediates Sema3E signaling and blood vessel development, we analyzed *plexin-D1* null mice (fig. S3). We observed little or no AP-Sema3E binding to sections prepared from *plexin-D1* null embryos (Fig. 2, J and K), indicating that plexin-D1 is essential for Sema3E binding. In contrast, we observed essentially identical AP-Sema3E binding to tissue sections prepared from wild-type embryos and embryos expressing a Npn-1 variant that binds to VEGF isoforms but not class 3 semaphorins [*npn-1*$^{Sema-/-}$ (*16*)] (Fig. 2, L and M). AP-Sema3A binding sites were, however, undetectable in sections prepared from *npn-1*$^{Sema-/-}$ mice (*15*, *16*). AP-Sema3E also bound to sections prepared from *npn-2*$^{-/-}$ embryos (*15*). The binding of Sema3E to plexin-D1 indicates that a Sema3 can associate directly with a plexin, independently of a neuropilin. We used a cell collapse assay (*17*) to assess whether Sema3E can signal through plexin-D1 in a neuropilin-independent manner. Treatment of plexin-D1–expressing COS-7 cells with Sema3E but not Sema3A induced collapse of lamellipodia (Fig. 3). Together, these findings indicate that plexin-D1 is the endogenous high-affinity receptor for Sema3E and that this ligand-receptor pair mediates cytoskeletal signaling and cell contraction independently of neuropilins.

We next determined whether ectopic expression of Sema3E affects blood vessel patterning in vivo. Sema3E was overexpressed in chick embryos by in ovo electroporation of expression vectors encoding Sema3E and green fluorescent protein (EGFP) into the somites. Embryonic vasculature was visualized after 48 hours with a rhodamine-conjugated lectin (LCA) solution (*18*). Few, if any, vessels were observed in areas of ectopic Sema3E expression (Fig. 3, K to N), whereas vascular patterning appeared normal in regions outside sites of ectopic Sema3E expression (Fig. 3, K to M). Electroporation of EGFP and the empty expression vector had no effect on vascular patterning or somite cytoarchitecture (Fig. 3, H to J, N). These experiments support the view that Sema3E expressed by somites acts as a repulsive cue to restrict vessel growth and branching to intersomitic regions during embryogenesis.

To address whether Sema3E is required in vivo for intersomitic vascular development, we analyzed *Sema3E* null mice (fig. S4). At E11.5, wild-type littermates displayed an iterative pattern of intersomitic blood vessels between each somite. In *Sema3E*$^{-/-}$ mutant embryos, however, intersomitic vessels were disorganized (Fig. 4, A to B′); vessels extended ectopically throughout somites, resulting in exuberant growth and a loss of the normal segmented pattern (n = 14

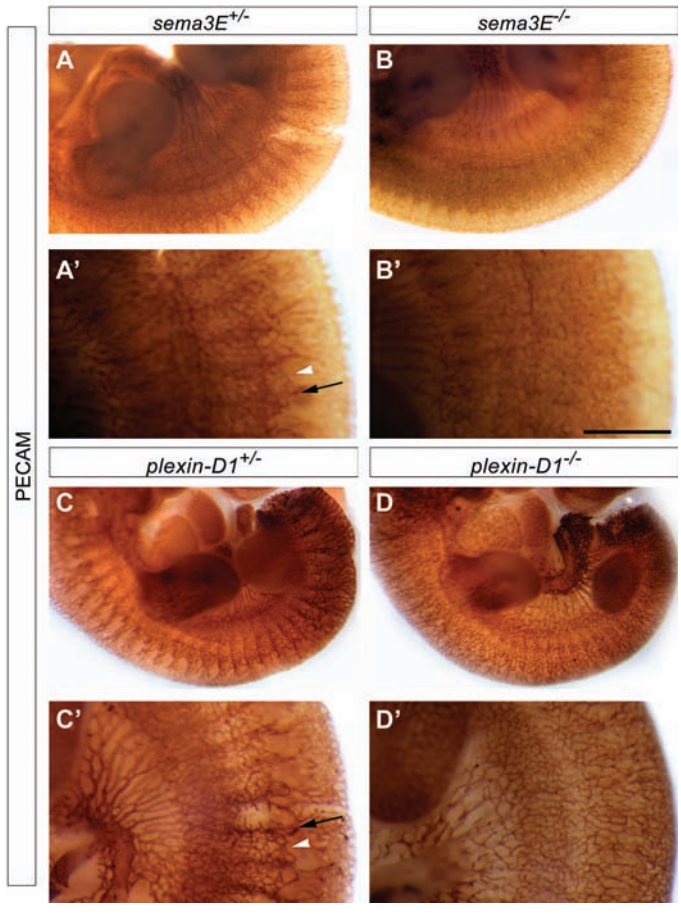

Fig. 4. Sema3E and Plexin-D1 are both required for intersomitic vascular patterning. (**A** and **B**) Whole-mount PECAM staining of E11.5 *sema3E*$^{+/-}$ (A) and *sema3E*$^{-/-}$ (B) mutant embryos showing a Sema3E requirement for normal organization of somitic vasculature. (**A′** and **B′**) High magnification views of E11.5 *sema3E*$^{+/-}$ (A′) and *sema3E*$^{-/-}$ (B′) embryos. The vascular phenotype was observed in all *sema3E*$^{-/-}$ mice (n = 14) but not in heterozygous (n = 4) or wild-type (n = 14) littermates. (**C** and **D**) PECAM staining of E11.5 control (C) and *plexin-D1*$^{-/-}$ mutant (D) embryos showing marked disorganization of somitic vasculature in the absence of plexin-D1 embryos, similar to *sema3E*$^{-/-}$ embryos. (**C′** and **D′**) High-magnification views of E11.5 control (C′) and *plexin-D1*$^{-/-}$ mutant (D′) embryos. The vascular phenotype was observed in all *plexin-D1*$^{-/-}$ mice (n = 8) but not in heterozygous (n = 8) or wild-type littermates (n = 8). White arrowhead, caudal somite; black arrow, intersomitic vessels. Scale bar, 1.2 mm [(A), (B), (C), and (D)]; 0.6 mm [(A′), (B′), (C′), and (D′)].

Sema3E mutants and 14 littermate controls). This phenotype was evident in mice bred into both CD1 and C57BL/6 genetic backgrounds (*15*) and is markedly similar to that observed in mice lacking plexin-D1 (Fig. 4, C to D′, and fig. S6). In *plexin-D1*$^{-/-}$ mice, the iterative pattern of somatic vascular organization was also abolished and vessels extended throughout each entire somite at both E10.5 and E11.5 (n = 8 E11.5 *plexin-D1*$^{-/-}$ mutants and 8 control littermates and n = 4 E10.5 *plexin-D1* mutants and 4 control littermates). This phenotype is comparable to that recently reported in another line of *plexin-D1*$^{-/-}$ mice (*10*) and in plexin-D1–deficient zebrafish (*11*).

The similarity in the nature and extent of vascular defects in *sema3E* and *plexin-D1* mutant mice suggests that somite-derived Sema3E serves as the ligand for plexin-D1 on endothelial cells in vivo. In zebrafish, vascular patterning has been suggested to result from signaling by Sema3A by means of a Npn-1/plexin-D1 complex. Nevertheless, knockdown of Sema3a1 or Sema3a2 resulted only in minor vascular defects that do not recapitulate the *plexin-D1* mutant phenotype (*11*). Conversely, mouse embryos lacking Sema3A show a modest decrease in intersomitic vessel branching (*8*) but, notably, this phenotype is incompletely penetrant and is not observed in all genetic backgrounds (*8*). To assess the in vivo contribution of neuropilins to Sema3E–plexin-D1 signaling, we generated *npn-1*$^{Sema-/-}$;*npn-2* double-mutant mice, in which the interactions between Sema3s and neuropilins are abolished (*15*–*19*). No vascular defect other than persistent truncus arteriosus (*16*) was observed in these mutant embryos (figs. S5 and S7) (*15*). Importantly, there was no difference in intersomitic vasculature between E10.5 and E11.5 *npn-1*$^{Sema-/-}$;*npn-2* double-mutant mice and control littermates (figs. S5 and S7). This finding further supports the view that Sema3E–plexin-D1 signaling is responsible for patterning intersomitic vasculature independently of neuropilins.

The discovery of an unanticipated neuropilin-independent Sema3 signaling pathway adds to the diversity of how Sema3s orchestrate tissue morphogenesis. A complementary pattern of expression of *Sema3E* and *plexin-D1* is also found in other regions of the developing embryo, most prominently the E13.5 forelimb and hindlimb digits, sites where vascular patterning defects are observed in *plexin-D1* mutants (*15*). Thus, Sema3E–plexin-D1 signaling may play a more general role in vascular patterning. Finally, both *Sema3E* and *plexin-D1* are expressed at many specific sites in the nervous system (*9*, *14*, *15*, *20*), and there is a strong association between the development of intersomitic blood vessels and spinal nerves (*21*). Thus, Sema3E–plexin-D1 signaling could also control aspects of neural development.

References and Notes

1. J. A. Raper, *Curr. Opin. Neurobiol.* **10**, 88 (2000).
2. A. B. Huber, A. L. Kolodkin, D. D. Ginty, J. F. Cloutier, *Annu. Rev. Neurosci.* **26**, 509 (2003).
3. Z. He, K. C. Wang, V. Koprivica, G. Ming, H. J. Song, *Sci. STKE* **2002**, re1 (2002).
4. T. Toyofuku *et al.*, *Genes Dev.* **18**, 435 (2004).
5. L. Tamagnone, P. M. Comoglio, *EMBO Rep.* **5**, 356 (2004).
6. S. Giordano *et al.*, *Nature Cell Biol.* **4**, 720 (2002).
7. M. L. Winberg *et al.*, *Cell* **95**, 903 (1998).
8. G. Serini *et al.*, *Nature* **424**, 391 (2003).
9. B. van der Zwaag *et al.*, *Dev. Dyn.* **225**, 336 (2002).
10. A. D. Gitler, M. Lu, J. A. Epstein, *Dev. Cell* **7**, 107 (2004).
11. J. Torres-Vazquez *et al.*, *Dev. Cell* **7**, 117 (2004).
12. S. Soker, S. Takashima, H. Q. Miao, G. Neufeld, M. Klagsbrun, *Cell* **92**, 735 (1998).
13. T. Kawasaki *et al.*, *Development* **126**, 4895 (1999).
14. N. Miyazaki *et al.*, *Neurosci. Res.* **33**, 269 (1999).
15. C. Gu *et al.*, unpublished data.
16. C. Gu *et al.*, *Dev. Cell* **5**, 45 (2003).
17. T. Takahashi *et al.*, *Cell* **99**, 59 (1999).
18. S. M. Jilani *et al.*, *J. Histochem. Cytochem.* **51**, 597 (2003).
19. C. Gu *et al.*, *J. Biol. Chem.* **277**, 18069 (2002).
20. J. Livet *et al.*, *Neuron* **35**, 877 (2002).
21. A. J. Levine, I. Munoz-Sanjuan, E. Bell, A. J. North, A. H. Brivanlou, *Dev. Biol.* **254**, 50 (2003).
22. We thank X. Chen, C. Deppmann, C.-M. Fan, J. Pasterkamp, and T. Pietri for helpful comments on the manuscript; B. Tice, T. Hippe, F. Lauro, and N. Senant for excellent technical assistance; A. Chen for help with chick electroporation; B. Han for cell culture; M. Mendelsohn for generation of *plexin-D1* mice; T. Pietri, E. R. Rodriguez and X. Chen for help with figures; and H. Cremer and J. Sager for helpful discussions. This work was supported by INSERM, CNRS, Association Française contre les Myopathies (AFM), European Commission contract QLG3-CT-1999-00602, ARC and IRME (J.L.), Christopher Reeve Paralysis Foundation (CRPF GB2-0301-1) (C.G.), a Human Frontier Science Program Fellowship (Y.Y.), the Packard Center for Amyotrophic Lateral Sclerosis Research at Johns Hopkins (D.D.G. and A.L.K.), NIH grants CA23767-24 (T.M.J.) and MH59199-06 (D.D.G. and A.L.K.), and the Howard Hughes Medical Institute (T.M.J. and D.D.G.). T.M.J. and D.D.G. are investigators of the Howard Hughes Medical Institute. Molecular interaction data have been deposited in the Biomolecular Interaction Network Database with accession codes 183369, 183370, 183371, 183372, and 183373.

Supporting Online Material
www.sciencemag.org/cgi/content/full/1105416/DC1
Material and Methods
Figs. S1 to S7
References and Notes

20 September 2004; accepted 9 November 2004
Published online 18 November 2004;
10.1126/science.1105416
Include this information when citing this paper.